The 2009 IEEE/RSJ International Conference on
Intelligent Robots and Systems
October 11-15, 2009 St. Louis, USA

Kinematic Calibration of a Parallel Robot for Small Animal Biopsies

Myun Joong Hwang, Ozkan Bebek, Fan Liang, Baowei Fei and M. Cenk Cavusoglu

Abstract— **In biomedical research it is difficult to perceive tumors or cells and perform biopsies manually. Robotics technology can offer a reliable solution for accurate needle insertion. A novel 5 degrees of freedom (DOF) robot for inserting needles into small animal subjects was developed. The robot can realize dexterous alignment of the needle using two parallel mechanisms, and has a syringe mechanism to insert needles to subjects. Operations on small animals require high accuracy positioning during needle insertion. In this paper, kinematic calibration of the 5 DOF robot using an optical tracker as an external sensor is performed to enhance accuracy of the system.**

I. Introduction

Small animals are used in various applications for biomedical research, but in most cases, small animals are used to develop drugs or therapies before they are used to treat human diseases. Manual needle insertion is time consuming and most of the time target tissues cannot be reached due to their small sizes.

Small animals have compact anatomy and tiny organs. It is difficult to perceive tumors or cells and perform biopsies manually. Therefore, image guided needle insertion has been preferred for its accuracy and safety [1]. For purposes of needle insertion, researchers have used X-ray computed tomography (CT) [2], magnetic resonance (MR) imaging [3], micro positron emission tomographic (PET) [3], [4], and ultrasound imaging [5], [6]. In these studies, the needle insertion trajectories to be followed were planned based on pre-operated images. In addition, intra-operative image guidance was used to confirm the position of the needle. Even though image guidance is helpful during needle insertion, it is difficult to manually insert the needle to the small sized target.

Inaccurate needle positioning can destroy cells and organs, and can even cause trauma. In cases of insertion failures or missed targets a new animal is used to repeat the experiment. Therefore, accuracy is an important factor in these experiments. Robotic-assisted autonomous needle insertion offers a convenient and reliable solution to this accuracy problem. Base on the nature of the problem the robot is required to have a light structure and should have high resolution and accuracy.

There are several studies on image guided robotic systems for small animal research which focuses on the development of robots [2]–[4], [7]. They usually used industrial robot [2] where in some the needle orientation was constrained [3], [4]. But, needle insertion to small animals cannot be accomplished with a simple vertical insertion since organs or bones can be in between the entry point and the target point. Therefore, various orientations should be considered for convenient needle positioning. Needle positioning error, including positioning error and system calibration error, should be below 1 mm to precisely reach target points such as tumors. Therefore, the first step of developing a robotic system for small animal biopsies is achieving high accuracy in the autonomous needle insertion.

We proposed a compact robot design to insert needles to small animal subjects in [8]. Parallel mechanisms are used for stable and reliable operation. The robot is operational and has 5 degrees of freedom (DOF) with two gimbal joints that carry a needle mechanism. The robot can realize dexterous alignment of the needle before insertion. The design is light weight, and has high position resolution.

Any error in kinematics may cause inaccurate movement. In the literature, kinematic calibrations are performed on robots by measuring actual robot position with external sensors or placing robots to fixtures. In medical application, even the slightest position errors might cause harm to the subjects. Therefore, accurate kinematic parameters should be found to improve accuracy of the surgical robots. Beasley *et al.* presented a kinematic error correction method based on the error for the Jacobian matrix of a minimally invasive surgical robot [9]. Chung *et al.* presented a calibration method using optical tracker in macro-micro surgical robotic system [10]. Chung's work is based on the calibration of Denavit-Hatenberg (D-H) parameters.

The objective of this paper is to validate accuracy of the robotic system after calibration. The robotic system consists of two parallel mechanisms and a syringe mechanism to insert needles to subjects. Robot's actuated joints are driven by tendon mechanisms. There are slight differences in the calculated and the actual transmission ratio (or gear ratio). Also there are offsets in the joint angles affected from initial starting position of the system. Distance and alignment of the front and back stage also should be measured precisely for accurate forward kinematics implementation. Therefore, we presented a method to compute transmission ratios, angle offsets of each actuated joint from their actual position, and constant lengths in the robot's frame. This kinematic calibra-

This work was supported in part by the National Science Foundation under grants CISE CNS-0423253, IIS-0805495 and IIS-0905344, US DoC under grant TOP-39-60-04003, and by the Korea Research Foundation Grant funded by the Korean Government (MOEHRD) under grant KRF-2007-357-D00012.

M. Cenk Cavusoglu, Ozkan Bebek, Myun Joong Hwang, and Fan Liang are with the Department of Electrical Engineering and Computer Science, Case Western Reserve University, Cleveland, Ohio, 44106, USA. cavusoglu@case.edu, oxb6@case.edu, mjh92@case.edu, fxl84@case.edu

Baowei Fei is with the Emory University School of Medicine, Atlanta, Georgia, 30322, USA. bfei@emory.edu

tion is performed on the robot by measuring actual position and orientation of robots extremities using an external sensor.

In Section II the specifics of the developed robotic system is given. The calibration process is explained and results are shown in Section III. Experimental results and concluding remarks are presented in Section IV and V, respectively.

II. Robotic System

Design requirements for the Small Animal Biopsy Robot were presented in detail in [8]. The robot design is briefly explained here to provide a complete view of the system. The robotic system should be able follow a desired insertion and extraction trajectory to perform operations on small animals. To accomplish this, the robotic system should have at least 5 DOF and realize various needle position configurations with high accuracy. Developed robotic system is shown at its zero configuration in Figure 1. The robot consists of three main parts, front stage, back stage and syringe mechanism.

Front stage has a 2 DOF parallel mechanism with a gimbal joint attached to its end effector. The gimbal joint is to support the needle. Back stage has the same 2 DOF parallel mechanism, in addition an extra 1 DOF is placed to rotate the parallel mechanism from its base. This additional freedom is to insert needle to the tissue. A mechanism to carry a syringe with needle was attached to the end effector of the back stage. Parallel mechanism, which is a 5-bar linkage, provides stable guiding of the needle. One of the advantages of the 5-bar linkage mechanisms is that bulky parts, such as motors, can be positioned at the base. This provides lighter links.

In the 5-bar mechanism, links attached to the base are actuated with a tendon-driven mechanism, where a capstan pulls the tensioned cable that rotates the disk around its axis. This transmission provides low friction motion without slipping or binding. Two different sized motors are used to drive the tendon-driven mechanisms. Maxon RE-25 Motors with 500 counts per turn (CPT) encoders are used to drive the front and back stage 5-bar mechanisms.The additional axis of the back stage is driven by a Maxon RE-30 Motor with 1000 CPT encoder [11]. Depending on the orientation of the 5-bar mechanisms, a position resolution of 5-50 μm is achievable with these position encoders.

The syringe mechanism has a Maxon RE-10 motor with gear head and encoder to operate the syringe plug (Figure 2). The mechanism is attached to the back stage end effector with a gimbal joint to allow free rotation. After the needle insertion is accomplished, the duty of the syringe mechanism is to deliver drugs or to collect samples from the animal.

A. Forward Kinematics

To find position of needle tip we derived the forward kinematics of robot system. Assigned coordinate frames of the robot are shown in Figure 3. l_f and l_b are link lengths of front stage and back stage, respectively. l_{fe} and l_{be} are link lengths between 5-bar-linkage end effector and gimbal joints of front stage and back stage, respectively. Distance between origin of front stage and that of back stage is denoted as d_{fb}.

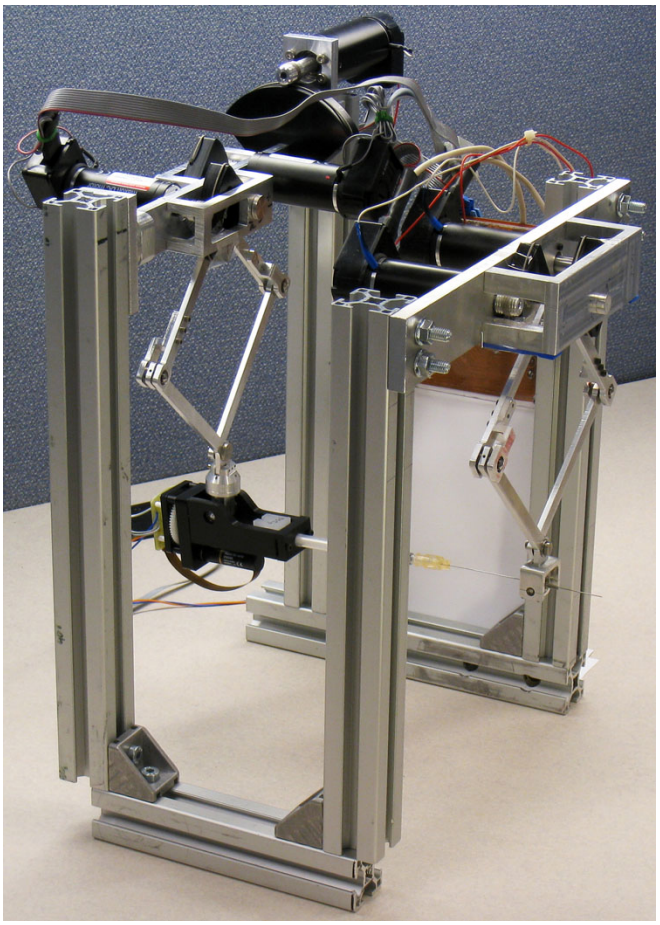

Fig. 1. 5 DOF Small Animal Drug Delivery/Biopsy Robot shown at its zero configuration.

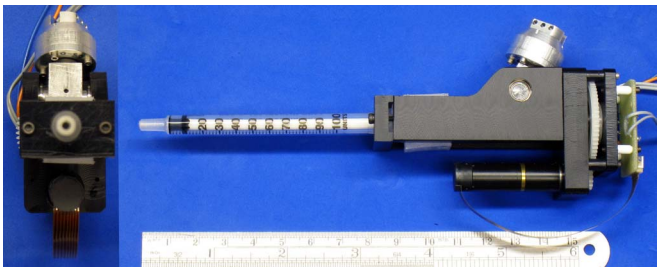

Fig. 2. Syringe mechanism designed to inject drugs or to retract samples using a needle.

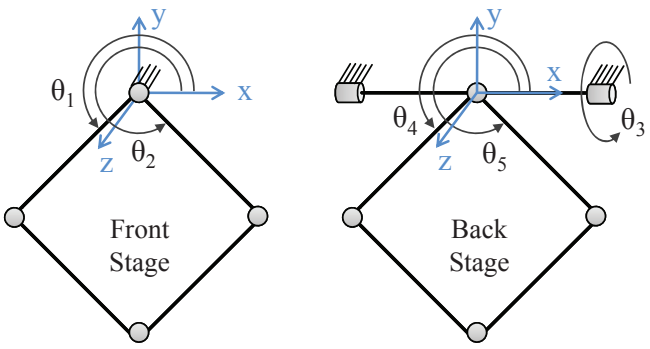

Fig. 3. Coordinate frames assigned to robot's front and back stages.

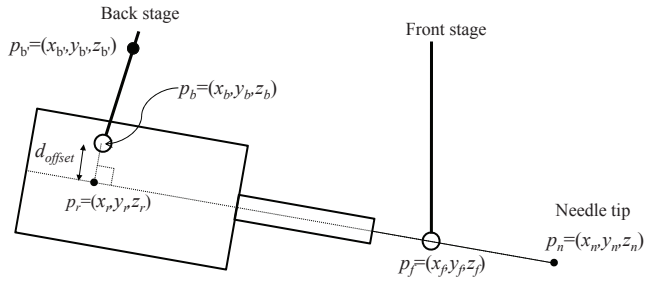

Fig. 4. Coordinate points on the syringe mechanism used in the derivation of robot's forward and inverse kinematics.

End effector positions of front and back stage are given in (1) and (2).

$$\begin{bmatrix} x_f \\ y_f \\ z_f \end{bmatrix} = \begin{bmatrix} (l_f\cos(\theta_1) + l_f\cos(\theta_2) + l_{fe}\cos(\theta_2 - \frac{\pi}{4}) \\ l_f\sin(\theta_1) + l_f\sin(\theta_2) + l_{fe}\sin(\theta_2 - \frac{\pi}{4}) \\ d_{fb} \end{bmatrix} \quad (1)$$

$$\begin{bmatrix} x_b \\ y_b \\ z_b \end{bmatrix} = \begin{bmatrix} l_b\cos(\theta_4) + l_b\cos(\theta_5) + l_{be}\cos(\theta_5 - \frac{\pi}{4}) \\ (l_b\sin(\theta_4) + l_b\sin(\theta_5) + l_{be}\sin(\theta_5 - \frac{\pi}{4}))\cos(\theta_3) \\ (l_b\sin(\theta_4) + l_b\sin(\theta_5) + l_{be}\sin(\theta_5 - \frac{\pi}{4}))\sin(\theta_3) \end{bmatrix} \quad (2)$$

Figure 4 shows the assigned coordinates of the syringe mechanism. $p_n = (x_n, y_n, z_n)$ is position of the needle tip. Distance between $p_b = (x_b, y_b, z_b)$ and extension line of needle is d_{offset}. $p_{b'} = (x_{b'}, y_{b'}, z_{b'})$ is the point of the joint in the back stage which is connected to syringe mechanism. $p_f = (x_f, y_f, z_f)$ is the crossing point of the needle from the front stage gimbal joint center. $p_r = (x_r, y_r, z_r)$ is crossing point on the extension line of needle. l_n is the sum of syringe mechanism length and needle length.

All points are placed on the same plane. Therefore, one can find a plane coinciding these three known points, which are p_f, p_b and $p_{b'}$. p_r is also on the same plane, hence it satisfies equation of plane as

$$Ax_r + By_r + Cz_r + D = 0 \quad (3)$$

$$A = \begin{vmatrix} 1 & y_b & z_b \\ 1 & y_{b'} & z_{b'} \\ 1 & y_f & z_f \end{vmatrix}, \quad B = \begin{vmatrix} x_b & 1 & z_b \\ x_{b'} & 1 & z_{b'} \\ x_f & 1 & z_f \end{vmatrix},$$
$$C = \begin{vmatrix} x_b & y_b & 1 \\ x_{b'} & y_{b'} & 1 \\ x_f & y_f & 1 \end{vmatrix}, \quad D = -\begin{vmatrix} x_b & y_b & z_b \\ x_{b'} & y_{b'} & z_{b'} \\ x_f & y_f & z_f \end{vmatrix}$$

Line between p_b and p_r is perpendicular to line between p_f and p_r, therefore

$$(p_b - p_r)\cdot(p_f - p_r) = 0, \quad (4)$$

and the distance between p_r and p_b is

$$(p_r - p_b)\cdot(p_r - p_b) = d^2_{\text{offset}}. \quad (5)$$

p_r satisfies (3-5) at the same time and it can be found by solving these three equations. From Figure 4, note that p_f, p_r and p_n are placed on the same line. Equation of this line is represented as in (6) using parameter t.

$$\frac{x_n - x_r}{x_f - x_r} = \frac{y_n - y_r}{y_f - y_r} = \frac{z_n - z_r}{z_f - z_r} = t \quad (6)$$

Distance between p_r and p_n is l_n as (7). Finally, p_n is found in (8) by replacing t in (6) with (7).

$$(p_n - p_r)\cdot(p_n - p_r) = t^2((p_f - p_r)\cdot(p_f - p_r)) = l_n^2 \quad (7)$$

$$p_n = t(p_f - p_r) + p_r \quad (8)$$

where

$$t = \frac{l_n}{\sqrt{(x_f - x_r)^2 + (y_f - y_r)^2 + (z_f - z_r)^2}}.$$

B. Inverse Kinematics

We also need to derive inverse kinematics in order to find joint angles from desired needle position, p_n, and orientation of needle tip. Let ${}^B_N R$ be the rotation matrix of needle with respect to robot base frame $\{B\}$. Then, p_b and p_r can be found from (9-10) using d_{offset} and l_n. Also, p_f can be solved from the line equation given in (11). Joint angles are derived from (9) and (11) using inverse kinematics of front stage and back stage, respectively. The results are shown in (12).

$$p_b = {}^B_N R \begin{bmatrix} 0 \\ d_{\text{offset}} \\ -l_n \end{bmatrix} + p_n \quad (9)$$

$$p_r = {}^B_N R \begin{bmatrix} 0 \\ 0 \\ -l_n \end{bmatrix} + p_n \quad (10)$$

$$p_f = \frac{d_{fb} - z_r}{z_n - z_r}(p_n - p_r) + p_r \quad (11)$$

$$\begin{aligned} \theta_1 &= atan_2(n_{2f}, n_{1f}) + \theta_2 \\ \theta_2 &= atan_2(c_f, -\sqrt{1 - c_f^2}) - atan_2(a_f, b_f) \\ \theta_3 &= atan_2(-z_b, -y_b) \\ \theta_4 &= atan_2(n_{2b}, n_{1b}) + \theta_5 \\ \theta_5 &= atan_2(c_b, -\sqrt{1 - c_b^2}) - atan_2(a_b, b_b) \end{aligned} \quad (12)$$

where $k_f = \frac{l_{fe}}{\sqrt{2}}$, $m_f = l_f + k_f$, $a_f = 2m_f x_f - 2k_f y_f$,
$b_f = 2k_f x_f + 2m_f y_f$, $c_f = \frac{x_f^2 + y_f^2 + 2m_k k_f}{\sqrt{a_f^2 + b_f^2}}$,
$n_{1f} = x_f\cos(\theta_2) + y_f\sin(\theta_2) - l_f - k_f$,
$n_{2f} = -x_f\sin(\theta_2) + y_f\cos(\theta_2) + k_f$
$y_{b2} = \frac{y_b}{\cos(\theta_3)}$, $k_b = \frac{l_{be}}{\sqrt{2}}$, $m_b = l_b + k_b$,
$a_b = 2m_b x_b - 2k_b y_{b2}$, $b_b = 2k_b x_b + 2m_b y_{b2}$,
$c_b = \frac{x_b^2 + y_{b2}^2 + 2m_b k_b}{\sqrt{a_b^2 + b_b^2}}$,
$n_{1b} = x_b\cos(\theta_5) + y_{b2}sin(\theta_5) - l_b - k_b$,
$n_{2b} = -x_b sin(\theta_5) + y_{b2}\cos(\theta_5) + k_5$

III. Kinematic Calibration

Kinematic calibration is the process to find errors in kinematic parameters. Kinematic calibration parameters include link length, link offset, joint angle offset, and so on which are D-H parameters in most serial manipulators. In our robotic system, we assume that each link in the parallel mechanism has no kinematic error since these links are manufactured at a high tolerance CNC machine. The robot has tendon-driven mechanisms to drive its actuated joints. The transmission ratio at these joints has uncertainty due to difficulty in measuring accurate ratio between encoder angle and joint angle. Motor encoders used are incremental type optical encoders; therefore joint angles have initial offset errors every time system is started. Gear ratio and joint angle offset are selected as calibration parameters, and denoted as GR_i and $\theta_{i,\text{offset}}$, respectively for the ith motor. Also, the distance between base links of front stage and back stage is determined since there can be alignment offsets between the two.

To identify calibration parameters, it is necessary to measure actual position of robot using an accurate sensor. In this research, an optical tracker system, NDI Polaris Vicra, is used as the external sensor. Polaris Vicra can measure 6 DOF position and orientation using optical marker tools. Sensor's accuracy is 0.25 mm RMS [12]. The optical marker tools are attached to the base of robot and end point of front and back stage to measure position and orientation of each stage as shown in Figure 5. Coordinate frames of the calibration setup is shown in Figure 6. $\{Bf\}$ and $\{Bb\}$ refer to the front and back stage coordinate frames attached to each stage's base joint center. $\{M\}$, $\{Tf\}$ and $\{Tb\}$ are the coordinate frames of the optical marker tools' origins defined by the manufacturer; and $\{S\}$ represents coordinate frame of the optical sensor. Therefore, ${}^S_{Tf}T$, ${}^S_{Tb}T$ and ${}^S_MT$ are homogeneous transformations with respect to optical tracker's coordinate frame, $\{S\}$.

The data from optical tracker and joint angles from encoders in the robot are matched by time stamp synchronization. Calibration process is represented in Figure 7. Front stage parameters and back stage parameters are calibrated separately in order to get a more accurate calibration.

First, the robot is moved to its physical limits and configuration data, ${}^S_MT$,${}^S_{Tf}T$ and ${}^S_{Tb}T$, are acquired. We choose to move the robot to its physical limits since this process can be repeated every time system is started. Encoder offsets can be reset at each system start, once the absolute encoder angles at the physical limits are determined. After the configuration data is transformed to the base frame of each robot using (13), each angle of ith joint, $\theta_{i,optIK}$, is computed using the inverse kinematics derived in Section II-B. These values are updated as starting encoder offsets.

During data collection in this calibration step, optical markers are kept at fixed positions and optical tracker base, which carries two fixed cameras, is kept moving around the optical markers. By averaging the collected data, error due to digitization of the image is minimized.

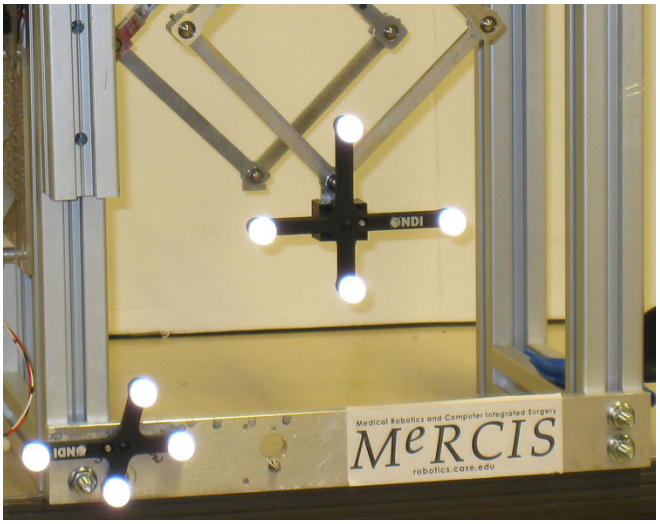

Fig. 5. Optical markers attached to the base of the robot and end effector of the 5-bar-linkage. The calibration for linkage mechanisms are done individually.

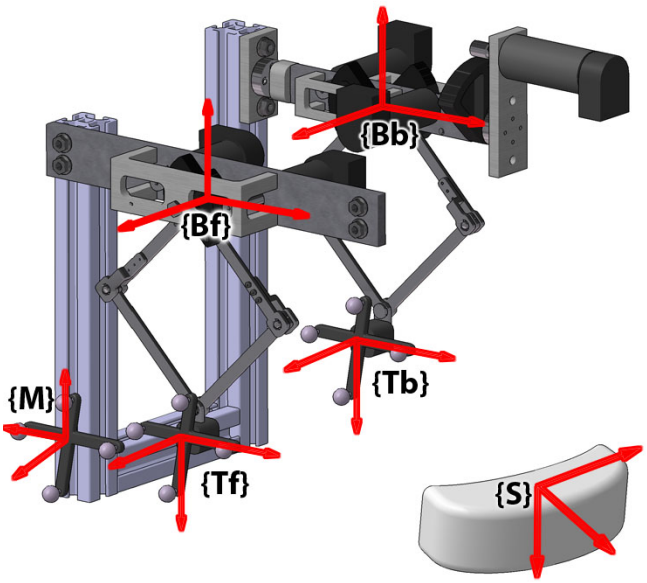

Fig. 6. Optical markers coordinates attached to the base of the robot and end effectors. $\{S\}$: Sensor, $\{M\}$: Base Marker, $\{Bf\}$: Front stage base, $\{Bb\}$: Back stage base, $\{Tf\}$: Front stage marker, $\{Tb\}$: Back stage marker.

$$ {}^{Bf}_{Tf}T = ({}^{Bf}_{M}T)({}^{M}_{S}T)({}^{S}_{Tf}T), \quad {}^{Bb}_{Tb}T = ({}^{Bb}_{M}T)({}^{M}_{S}T)({}^{S}_{Tb}T) \tag{13} $$

After the angles offsets are set, gear ratio, GR_i, is calibrated. GR_i is the transmission ratio between encoder angle of the ith motor and the ith joint angle (relation is shown in (14)).

$$ \theta_{i,enc} GR_i = \theta_{i,optIK} \tag{14} $$

In this calibration step, robot's front and back stages are made to follow a pre-determined trajectory. GR_i is computed using linear least squares by comparing the collected data

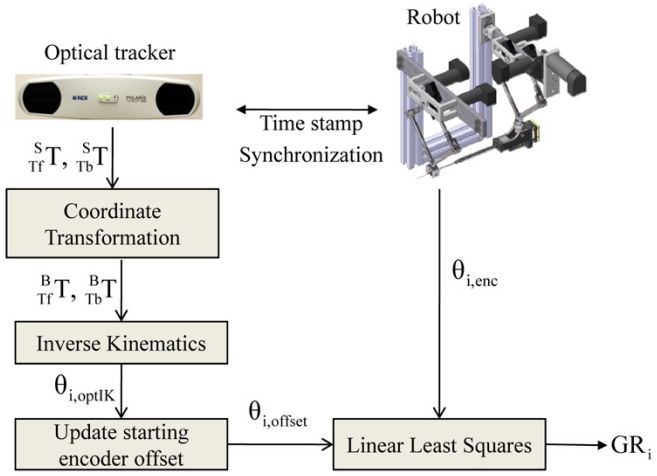

Fig. 7. Calibration method to find gear ratio, GR_i, and offset angle $\theta_{i,\text{offset}}$, of the ith joint.

from motor encoders and optical tracker.

$$GR_i = (a_i^T a_i)^{-1} a_i^T b_i \tag{15}$$

where, $a_i = \begin{bmatrix} \theta_{i,enc}(t_0) \\ \vdots \\ \theta_{i,enc}(t_n) \end{bmatrix}$, $b_i = \begin{bmatrix} \theta_{i,optIK}(t_0) \\ \vdots \\ \theta_{i,optIK}(t_n) \end{bmatrix}$.

When we attach the optical marker tools to the end points of each stage, orientation of the marker tools cannot be exactly matched to the base of robot. Therefore, we need to find mounting offsets that exist in the front stage and back stage. Mounting offsets are computed by comparing rotation matrices of each optical marker tool, ${}^{M}_{Tf}R$ and ${}^{M}_{Tb}R$, with orientation of each stage when robot is placed in its physically limited furthest position. The derived mounting offsets are denoted as ${}^{Tf}_{Tf'}R$ and ${}^{Tb}_{Tb'}R$. If the distance between the origin of optical marker tools and origin of end effectors are given, ${}^{Tf}_{Tf'}T$ and ${}^{Tb}_{Tb'}T$ can be found. Then, base frame of each stage can be represented as ${}^{M}_{Bf}T$ and ${}^{M}_{Bb}T$ using (16). The relation between base frame of front stage and that of back stage is derived in (17).

$$ {}^{M}_{Bf}T = ({}^{M}_{S}T)({}^{S}_{Tf}T)({}^{Tf}_{Tf'}T)({}^{Tf'}_{Bf}T) \tag{16}$$

$$ {}^{M}_{Bb}T = ({}^{M}_{S}T)({}^{S}_{Tb}T)({}^{Tb}_{Tb'}T)({}^{Tb'}_{Bb}T)$$

$$ {}^{Bb}_{Bf}T = ({}^{M}_{Bb}T)^{-1}({}^{M}_{Bf}T) \tag{17}$$

Forward kinematics equation (1) given in Section II-A is updated as (18), so that all end effector positions are represented in the back stage base, $\{Bb\}$, frame.

$$\begin{bmatrix} x_f \\ y_f \\ z_f \end{bmatrix} = {}^{Bb}_{Bf}T \begin{bmatrix} (l_f \cos(\theta_1) + l_f \cos(\theta_2) + l_{fe} \cos(\theta_2 - \frac{\pi}{4}) \\ l_f \sin(\theta_1) + l_f \sin(\theta_2) + l_{fe} \sin(\theta_2 - \frac{\pi}{4}) \\ 0 \end{bmatrix} \tag{18}$$

Similarly, inverse kinematics equation (11) given in Section II-B is updated as in (19) to get the front stage gimbal joint center coordinates with respect to front stage base, $\{Bf\}$, frame.

$$p_f = ({}^{Bb}_{Bf}T)^{-1} \frac{d_{fb} - z_r}{z_n - z_r}(p_n - p_r) + p_r \tag{19}$$

Even though needle tip position can be computed using forward kinematics equations (18), (2), and (17) with acquired joint angles, the error in measurement of l_n (defined in (7)) can cause inaccuracies in the needle tip position. In order to find the actual needle length, a single optical sphere is attached at the needle tip and position data is recorded while the robot followed a predetermined trajectory. This last external measurement is used to find the actual l_n.

IV. Experimental Results

We tested our calibrated system by attaching a pencil to the syringe mechanism instead of a needle. Pencil's tip thickness is 0.5 mm. A white paper is placed in front of the robot so that the needle is positioned normal to the paper when the robot is at its zero configuration. While maintaining pencil tip's contact on a white paper, robot is moved along a straight line. Drawn straight line length on the paper is compared to the line length derived from the forward kinematics. This process is repeated several times and an average position error is determined to be 2 mm.

V. Concluding Remarks

In this paper we presented the calibration method used on the 5 DOF parallel robot designed for inserting needles to small animal subjects. Before calibration, accuracy of the system was tested to be around 5 mm. We performed the calibration in multiple steps to achieve higher accuracies. Total of 15 parameters are calibrated. Using the calibrated system we showed that the system can achieve an end effector position accuracy of 2 mm. Parallel manipulators with similar position accuracies are reported in the literature [13]. Despite that the accuracy of the robot presented here is slightly above the required sub-millimeter accuracy for injecting needles to target positions, one should note that accuracy of the system would improve under real-time intra-operative image guidance.

References

[1] K. Cleary, A. Melzer, V. Watson, G. Kronreif, and D. Stoianovici, "Interventional robotic systems: Applications and technology state-of-the-art," *Minimally Invasive Therapy*, vol. 15, no. 2, pp. 101–113, 2006.

[2] A. Ayadi, G. Bour, M. Aprahamian, B. Bayle, P. Graebling, J. Gangloff, L. Soler, J. M. Egly, and J. Marescaux, "Fully automated image-guided needle insertion: Application to small animal biopsies," in *Proceedings of the 29th Annual International Conference of the IEEE EMBS*, Lyon, France, 8 2007, pp. 194–197.

[3] Y. H. Huang, T. H. Wu, M. H. Lin, C. C. Yang, W. Y. Guo, Z. J. Wang, C. L. Chen, and J. S. Lee, "An automated robot arm system for small animal tissue biopsy under dual-image modality," *Nuclear Instruments and Methods in Physics Research Section A: Accelerators, Spectrometers, Detectors and Associated Equipment*, vol. 569, no. 2, pp. 230–234, December 2006.

[4] P. Kazanzides, J. Chang, I. Iordachita, J. Li, C. C. Ling, and G. Fichtinger, "Development of an image-guided robot for small animal research," *Computer Aided Surgery*, vol. 12, no. 6, pp. 357–365, November 2007.

[5] P. Abolmaesumi, S. Salcudean, W. Zhu, M. Sirouspour, and S. DiMaio, "Image guided control of a robot for medical ultrasound," *IEEE Transactions on Robotics and Automation*, pp. 11–23, February 2002.

[6] A. C. Waspe, J. C. Lacefield, and A. Fenster, "Registration of three-dimensional high-frequency ultrasound images to a robotic needle-positioning system for preclinical research," in *4th IEEE International Symposium on Biomedical Imaging: From Nano to Macro (ISBI)*, April 2007, pp. 1132–1135.

[7] A. C. Waspe, H. J. Cakiroglu, J. C. Lacefield, and A. Fenster, "Design, calibration and evaluation of a robotic needle-positioning system for small animal imaging applications," *Physics in Medicine and Biology*, vol. 52, no. 7, pp. 1863–1878, 2007.

[8] O. Bebek, M. J. Hwang, B. Fei, and M. C. Cavusoglu, "Design of a small animal biopsy robot," in *Proceedings of the 30th Annual International Conference of the IEEE Engineering in Medicine and Biology Society (EMBC)*, Vancouver, British Columbia, Canada, August 2008, pp. 5601 – 5604.

[9] R. A. Beasley, R. D. Howe, and P. E. Dupont, "Kinematic error correction for minimally invasive surgical robots," in *Proceedings of the IEEE International Conference on Robotics and Automation*, 2004, pp. 358–364.

[10] J. H. Chung, B.-J. Y. S. Kim, W. K. Kim, Y. S. Kim, and S. H. Oh, "Accuracy enhancement of a surgical robot system using a bi-planar fluoroscopy," in *Proceedings of the 39th International Symposium on Robotics*, Seoul, Korea, October 2008, pp. 894–899.

[11] Maxon, *RE-30 60 Watt and RE-25 10 Watt Precious Metal Brushes DC Motors*, Maxon Precision Motors Inc., Fall River, MA, USA, 2009. [Online]. Available: http://www.maxonmotor.com

[12] NDI, *Polaris Vicra Optical Tracker System*, Northern Digital Inc., Waterloo, Ontario, Canada, 2009. [Online]. Available: http://www.ndigital.com/medical/polarisfamily-techspecs.php

[13] H. Liao, K. Yoshimura, T. Utsugida, K. Matsumiya, K. Masamune, and T. Dohi, "Surgical manipulator with linkage mechanism for anterior cruciate ligament reconstruction," in *Proceedings of the IEEE/RSJ International Conference on Robots and Systems*, San Diego, CA, USA, October-November 2007, pp. 1266–1271.